4-2015

An Aerodynamic Simulation of Disc Flight

Erynn J. Schroeder
College of Saint Benedict/Saint John's University

An Aerodynamic Simulation of Disc Flight

An Honors Thesis

College of St. Benedict/St. John's University

In Partial Fulfillment of the Requirements for Distinction
in the Department of Physics

Erynn Schroeder
Advisor: Dr. Thomas Kirkman
April, 2015

An Aerodynamic Simulation of Disc Flight

Approved by:

____

Dr. Thomas Kirkman, Associate Professor of Physics

____

Dr. Jim Crumley, Associate Professor of Physics

____

Dr. Dean Langley, Professor of Physics

____

Dr. Dean Langley, Chair, Department of Physics

____

Dr. Emily Esch, Director, Honors Thesis Program

Abstract

In this project, two disc flight simulations were created in Mathematica. The first predicted the flight trajectory of a disc in two dimensions based on angle of attack and initial velocity input parameters. The second simulation predicted flight more accurately in three dimensions, taking the torque into account and showing the roll at the end of long flights. Equations for the simulations came from the forces known to act on flying objects as well as coefficient functions for lift, drag, and torque roll moment. Fundamental aerodynamic properties and flight patterns of Discraft Ultra-Star flying discs were measured with the use of video recording and an onboard flight data recorder for comparison with the results of each simulation.

Introduction

History:

Flying discs, more commonly known as Frisbees, have fascinated people for millennia. The name “Frisbee” originally comes from Frisbie’s pie tins (Fig. 1a), first thrown by Connecticut schoolchildren and Yale students in the late 1800s. However, Frisbee-like objects have been used for much longer. For example, the Olympic discus (Fig. 1c) was introduced c. 700 BC, and ancient Indian cultures used a disk-like spinning weapon called the chakram (Fig. 1b) c. 1500 (Scodary, 2007). Though the designs and shapes of a pie tin, discus, and chakram are quite different from today’s most popular sport disc, the motion is described by the same forces.

Following the tossing of Frisbie’s pie tins, a demand grew for better flying discs. Walter Frederick Morrison (Fig. 1d) started the first injection mold production in the late 1940s, but his model was notorious for shattering on impact with any hard surface. Rich Knerr and A. K. Melin of Wham-O created an improved model (Fig. 1e) in 1957 based on Morrison’s design. (Potts & Crowther, 2002) The sport of ultimate was devised in 1969 and is now played competitively worldwide. Another disc sport, disc golf (Fig 1f), was devised in the early 1900s (Wikipedia, 2015) and uses smaller, more dense versions of plastic discs, exploiting their high velocity, long flight characteristics.

(a) Frisbie's Pie Tin (Photobucket, 2015)

(b) Chakram (Sikhnet, 2015)

(c) Discus (Viresethonestas)

(d) Morrison's Pluto Platter (Mother Nature Network, 2015)

(e) Wham-O Frisbee (Boomer, 2015)

(f) Disc Golf chains (Washington & Lee, 2015)

Figure 1- Examples of the early thrown disc designs and applications.

Past work:

Previous studies of disc flight have been conducted using wind tunnels, video cameras, various disc shapes, computer simulations, and on-board data collectors. Several studies have used wind tunnels to collect data about the air flow around a disc, most notably Potts & Crowther (2000, 2001, 2002). In their 2002 experiment, a disc was held by a metal frame and connected to a motor for spin capability. The disc was outfitted with a pressure transducer connected to twenty pressure sensors on each side of the disc, allowing for measurements across the disc surface (fig. 2a and 2b).

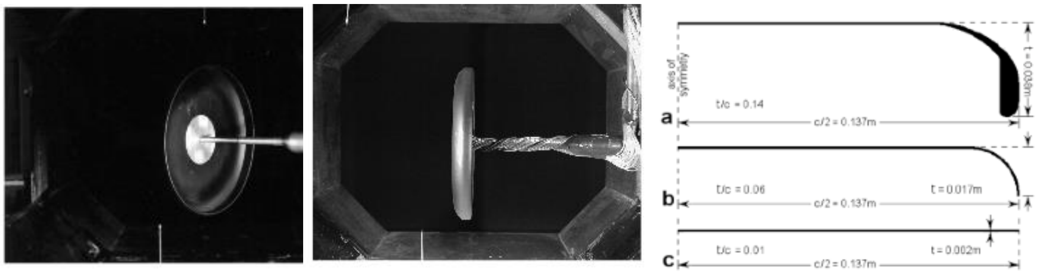

(a)Back view of rig configuration (b) Side view (c) Disc types

Figure 2 – Potts & Crowther (2010) setup for measurements in a wind-tunnel. The L-shaped configuration supports a vertical disc at a specific angle of attack for measurement of pressure distribution. Figure 2c shows the shapes of the three types of discs tested.

Conditions included constant wind velocities of 20 m/s while varying attack angles between -10 and 30 degrees; and a constant 5 degree angle of attack for wind speeds of 6, 10, 15 and 20 m/s. Three disc shapes were used: a flat plate, an intermediate shape and a normal disc (fig. 2c). It was determined that while flatter plates have less drag and more lift, the roll moment is also increased, giving a faster precession rate.

In the same study, Potts & Crowther created plots of the varying lift and drag coefficients with varying attack angle (fig 3). They found that lift and drag are largely unaffected by spin. This data has high validity, having been performed in a wind tunnel with measurable parameters (wind speed, attack angle, spin rate, etc).

Hubbard & Hummel (2000) explored flight characteristics through tracking flights with high speed cameras and creating a flight simulation. In their analysis, they used the lift and drag coefficient curves from the Potts and Crowther study. The lift coefficient and roll moment equations were approximated with linear dependence on attack angle; drag coefficient was approximated as a quadratic function of attack angle.

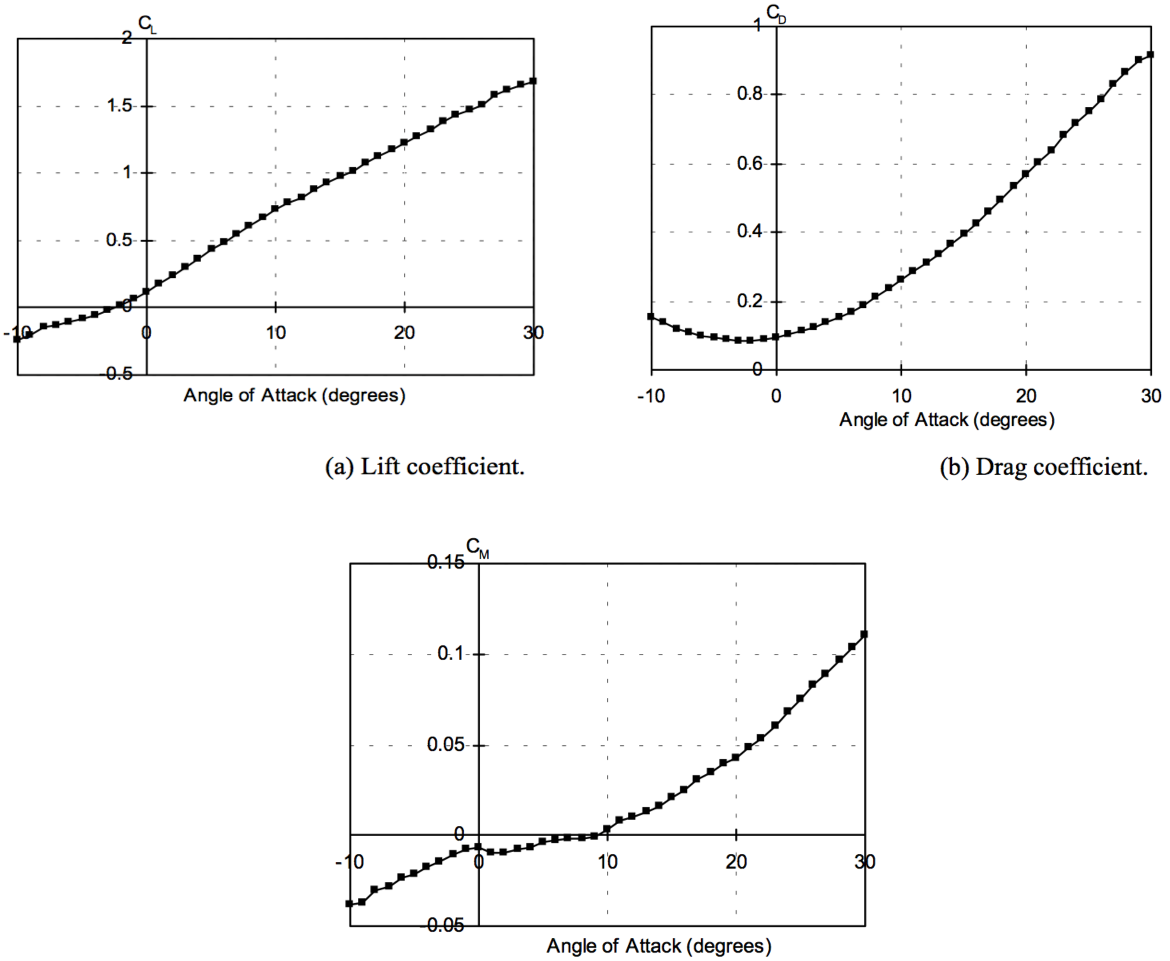

(a) Lift coefficient.

(b) Drag coefficient.

(c) Pitching moment coefficient.

Figure 3- Lift (a), drag (b), and pitch moment (c) coefficients from Potts & Crowther (2002).

Theory

As mentioned in the Potts & Crowther study, lift and drag are unaffected by spin, so in the most basic sense, a disc is like an airplane. The relevant forces in this simplified, two dimensional case, which assumes that the 'wing' of the disc remains level, are drag, lift, and gravity.

Gravity, $F_G = m * g$ is an always-present force pulling the disc back to earth. In the previous equation, m is the disc mass and g represents the gravitational constant. The pressure difference between the top and bottom of the disc while it flies create the lift and drag forces, which take the form: $F = \frac{1}{2}\rho v^2 AC(\alpha)$, where ρ is the density of air, v is the velocity of the disc compared to the ground, and A is the planform area of the disc . C is a coefficient related to each force. The directions of these forces can be seen below (Fig. 4). Drag opposes velocity, and lift is perpendicular to both.

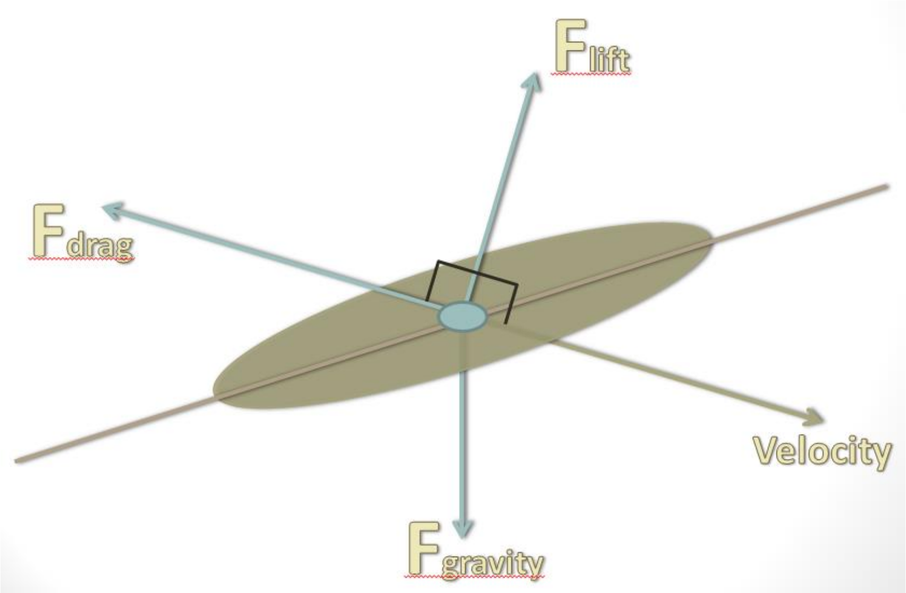

Figure 4- Forces on the disc.

Angle of attack, α, is measured as the direction of the disc velocity relative to the disc plane. It is important to note that while the angle of the disc relative to the ground may stay roughly constant, the angle of attack changes. At the end of the flight as the disc drops, the attack angle becomes large and both lift and drag are increased. In this two-dimensional approximation, the only variables which govern flight path are initial velocity and initial angle of attack.

Knowing the definition of angle of attack and that the drag force opposes velocity and lift is perpendicular, some vector manipulation gives the actual forces as:

$$F_L = \frac{1}{2}\rho A C_L(\alpha)\frac{(v \times n) \times v}{cos(\alpha)}$$

$$F_D = \frac{1}{2}\rho v|v| A C_D(\alpha)$$

$$sin(\alpha) = \left(\frac{-v \cdot n}{|v|}\right)$$

These equations use velocity defined as that of the disc in the space frame and n as the normal vector, perpendicular to the disc axis, also in the space frame.

The two-dimensional “airplane” approximation is not a poor one for short, straight flights, but in reality a third dimension is required. The 2D approximation assumes the orientation of the disc in space, corresponding to the $\hat{n}$ vector, does not change in flight. However, if a disc is tossed with no spin, it wobbles, catches the air, and does not travel straight. This motion is caused by the torque of the wind as it hits the underside of the disc. The torque acts to change the angular momentum, a phenomenon known as precession. To describe precession, angular momentum and torque must first be defined.

Angular momentum, L, depends only on the moment of inertia of the disc and the spin rate, ω_d. In the body fixed frame, this could be written as:

$$L = \begin{bmatrix} I_1 & 0 & 0 \\ 0 & I_2 & 0 \\ 0 & 0 & I_3 \end{bmatrix} * \omega_d$$

with $I_1 = I_2 = \frac{1}{2} I_3$ because the x and y axes of a round disc are symmetrical.

Torque is defined as the time rate of change in angular momentum.

$$\tau = \frac{dL}{dt}$$

Because there is a component of angular momentum which is constant in the disc frame, changes in angular momentum affect the actual orientation of the disc in space. This change in orientation is exemplified as a roll motion, known as precession. A simplified approximation of the rate of this precession for a fast-spinning gyroscope is:

$$Precession\,rate\colon \quad \omega_p = \frac{\tau}{L}$$

This suggests that discs thrown with more spin will have less precession, but all discs will precess. It also follows that a disc will continue to precess forever, completing whole circles in the roll direction, though this is not typically observed; thrown discs typically fall to Earth before completing a full roll rotation.

The orientation of a precessing gyroscope in space is best described with Euler angles (fig 5). They are used to describe a frame of reference, and in this case, they relate the space frame (of Earth) to the computational frame used in the simulations.

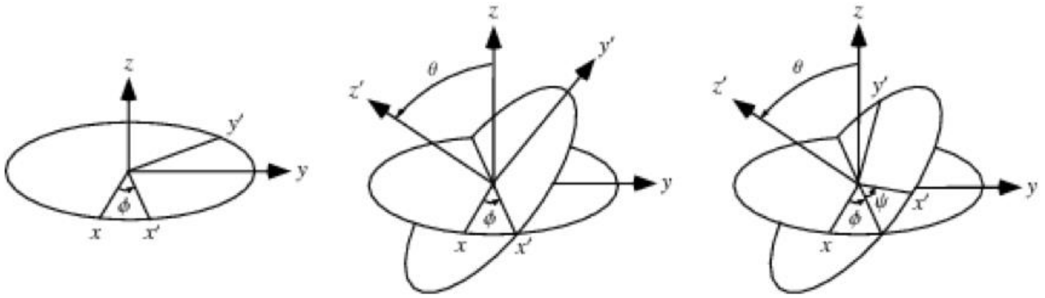

Figure 5- Euler angles. Note that in this diagram, the second rotation is around the x axis (Wolfram, 2015).

Only the first two rotations of Euler's construction define the computational frame. This frame moves with the disc through space, but the disc spins within the frame. Because the disc is rotationally symmetric, the x' y' and z' axes of this frame are still the principal axes. The first rotation is around the space z-axis by angle phi. The second rotation is around the new y-axis by angle theta:

$$phi\ matrix\ (first\ rotation): \qquad [\varphi] = \begin{bmatrix} \cos(\varphi(t)) & -\sin(\varphi(t)) & 0 \\ \sin(\varphi(t)) & \cos(\varphi(t)) & 0 \\ 0 & 0 & 1 \end{bmatrix}$$

$$theta\ matrix\ (second\ rotation): \quad [\theta] = \begin{bmatrix} \cos(\theta(t)) & 0 & \sin(\theta(t)) \\ 0 & 1 & 0 \\ -\sin(\theta(t)) & 0 & \cos(\theta(t)) \end{bmatrix}$$

Multiplying these together can transform a vector in the space frame to the computational frame.

Because the computational frame that we are using is itself precessing, the torque has an extra correction term (Taylor, 2005):

$$\tau = \frac{dL}{dt} + (\omega_f \times L)$$

This equation is fully general for calculating torque in a rotating frame. ω_f is the frame rotation rate, which in this case corresponds to precession rate of the disc.

The torque moment equation, which is based on a similar form to the drag and lift forces calculated earlier, is:

$$\tau = \frac{1}{2} A\rho |v| 2r \frac{v \times n}{cos(\alpha)} C_P(\alpha)$$

Inverse rotation matrices are used to transform the velocity vector to the computational frame which is then crossed into the normal vector, which is just (0, 0, 1) in the computational frame.

Procedure

The goal of this project was to model the flight of a Discraft Ultra-Star Sportdisc (fig. 6). These discs are said to weigh 175 grams and have a diameter of 10.75 inches (Discraft, 2015). My measurements of 6 multi-colored Ultra-Star discs gave an average weight of 174 ± 3 grams and diameter of 10.8 ± 0.3 inches. Other characteristics of these discs were measured through both video and onboard Flight Data Recorder analysis and used to create a simulation that estimates flight path.

Figure 6– Discraft Ultra-Star disc (Discraft, 2015).

Part 1: Video Recording and Analysis

For many elements of this project, data was collected and stored as video. These data were captured with a Canon VIXIA HF-M Series hand-held camcorder provided by the Saint John's University library. Individual clips were analyzed with the Tracker application program (Brown, 2015), which has the capability of storing data such as horizontal and vertical positions for each frame of the video. The camera captured frames every 33 milliseconds, or about 30 frames per second. Time-dependent positions were used to find both velocity and acceleration values.

One of the first tasks was to measure an Ultra-Star disc's moment of inertia, which was completed through comparison with objects of known inertial moments. Because a single disc does not roll straight, moment of inertia of a sport disc was found by placing two together and rolled down a ramp. Objects of known moments of inertia were rolled down the same ramp for comparison. The rolling was caught on camera and physical positions were analyzed in Tracker and fit with the Web-based Analysis Program for Physics (WAPP+) to find acceleration values for each object. The moment of inertia was determined by ratio of accelerations. As expected, the experimental inertial moment matched that of a uniform disk within error.

Videos were also taken of discs in flight. They were recorded in various locations (eg. behind St. Patrick hall, outside of the Peter Engel Science Center, and in the Bethel College and Clemens Field Houses) and again analyzed with Tracker (fig. 7). Tracker data was recorded for sixteen throws.

The two-dimensional dynamic position data from these videos was used to calculate drag and lift coefficients for the specific angles of attack captured. The attack angle range was small in our data, but the number of trials gave an estimate of the lift and drag coefficients for comparison with Potts & Crowther wind-tunnel data.

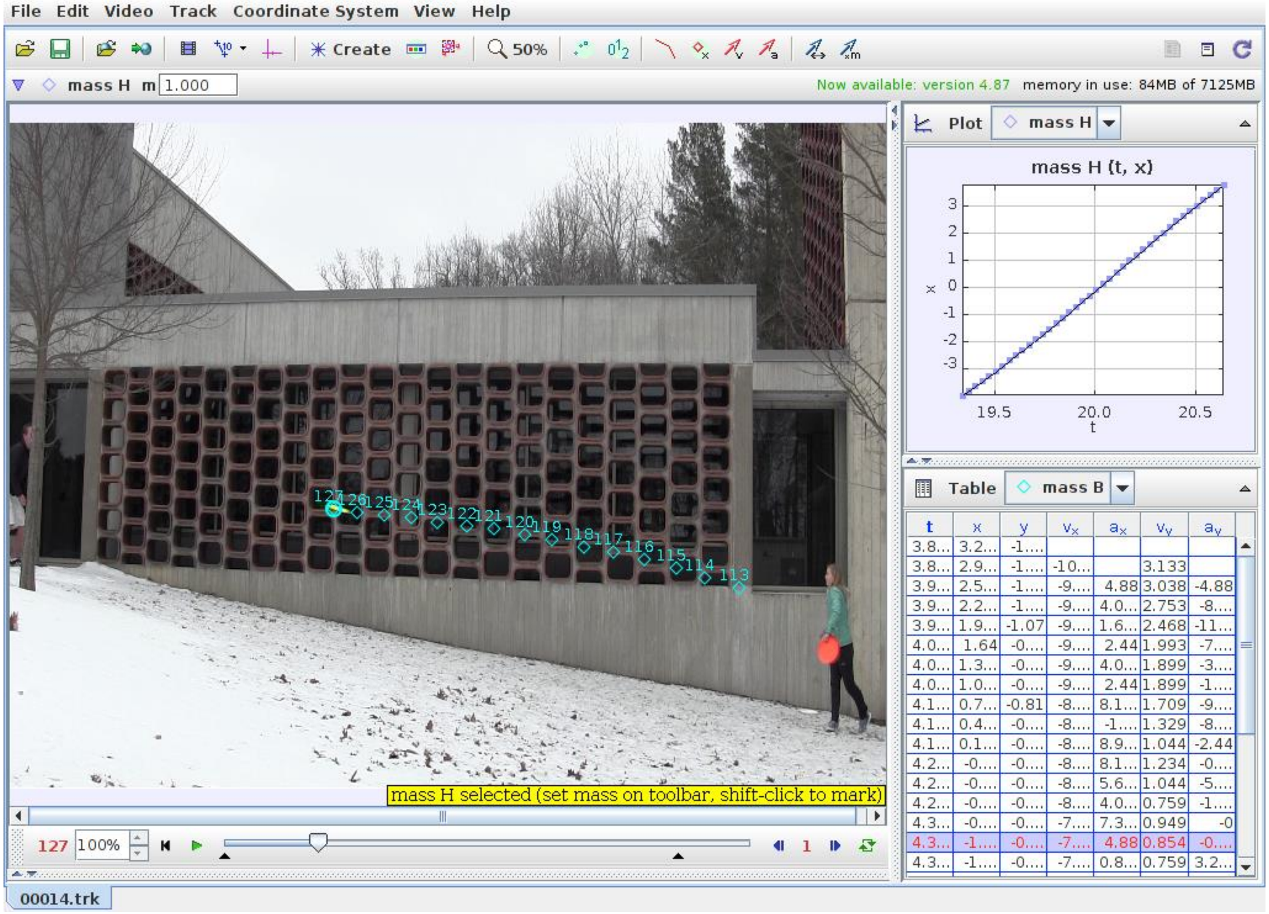
File Edit Video Track Coordinate System View Help
Create
50%
mass H m 1.000
Now available: version 4.87 memory in use: 84MB of 7125MB
Plot
mass H
mass H (t, x)
3
2
1
0
-1
-2
-3
x
19.5
20.0
20.5
t
127 126 125 124 123 122 121 120 119 118 117 116 115 114 113
mass H selected (set mass on toolbar, shift-click to mark)
127
100%
1
00014.trk
Table
mass B

t	x	y	v_x	a_x	v_y	a_y
3.8...	3.2...	-1....				
3.8...	2.9...	-1....	-10...		3.133	
3.9...	2.5...	-1....	-9....	4.88	3.038	-4.88
3.9...	2.2...	-1....	-9....	4.0...	2.753	-8....
3.9...	1.9...	-1.07	-9....	1.6...	2.468	-11...
4.0...	1.64	-0....	-9....	2.44	1.993	-7....
4.0...	1.3...	-0....	-9....	4.0...	1.899	-3....
4.0...	1.0...	-0....	-9....	2.44	1.899	-1....
4.1...	0.7...	-0.81	-8....	8.1...	1.709	-9....
4.1...	0.4...	-0....	-8....	-1....	1.329	-8....
4.1...	0.1...	-0....	-8....	8.9...	1.044	-2.44
4.2...	-0....	-0....	-8....	8.1...	1.234	-0....
4.2...	-0....	-0....	-8....	5.6...	1.044	-5....
4.2...	-0....	-0....	-8....	4.0...	0.759	-1....
4.3...	-0....	-0....	-7....	7.3...	0.949	-0
4.3...	-1....	-0....	-7....	4.88	0.854	-0....
4.3...	-1....	-0....	-7....	0.8...	0.759	3.2...

Figure 7- An example of a backhand throw tracked frame by frame on Tracker

Part 2: Flight Data Recorder

Further data was collected with an on-board flight data recorder (FDR). Dr. Thomas Kirkman put together the physical recording system and it was attached directly to the bottom of an Ultra-Star disc. The FDR is made of several components, including: a Teensy 3.1 Microcontroller, Adafruit 9-DOF IMU Breakout, a Lithium Ion Polymer Battery (3.7 V, 150 mA), and a MicroSD card breakout board.

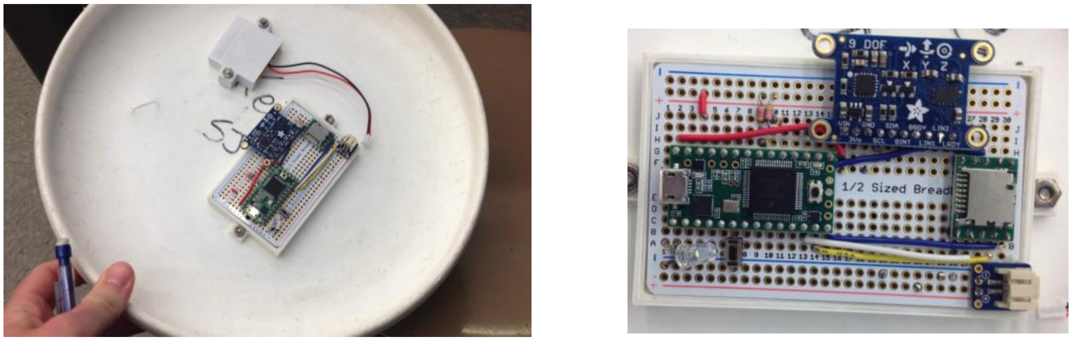

(a) The Flight Data Recorder and battery (b) A close-up of the FDR

Figure 8- The Flight Data Recorder, attached to the underside of an Ultra-Star, centered for mass distribution. Components included a Teensy 3.1 Microcontroller, Adafruit 9-DOF IMU Breakout, a Lithium Ion Polymer Battery, and a MicroSD card breakout board.

The FDR and battery were mounted the disc with 3D printed plastic boxes. Pieces were shaped and created with a 3D printer after being modeled with Computer-aided Design (CAD) (de Vries, 2013). The proportions necessary for the box were measured, then a prototype was drawn on paper before being converted to a 3D render and printed. The addition of this hardware to the Frisbee increased the mass by more than a third, with a final mass of 245.4 ± 0.1 grams. The FDR was centered well, allowing for level flight.

With the FDR was attached, data was collected while tossing the disc. The FDR functioned as a gyroscope, magnetometer, and accelerometer, and each of these parameters was measured in three dimensions, giving a total of nine degrees of freedom measured for each flight.

This data was collected every 23-24 milliseconds, so about 40 data points per second, for about 12.3 seconds for each trial and stored as text files on a Kingston SD chip. Trials were completed for a variety of throws, including backhand, forehand, push-pass, and hammer. For several trials, both video and FDR data were recorded. Comparing the FDR data to a visual record of the throw was helpful in comparing throws of multiple types. The two most common throws are shown here (fig. 9).

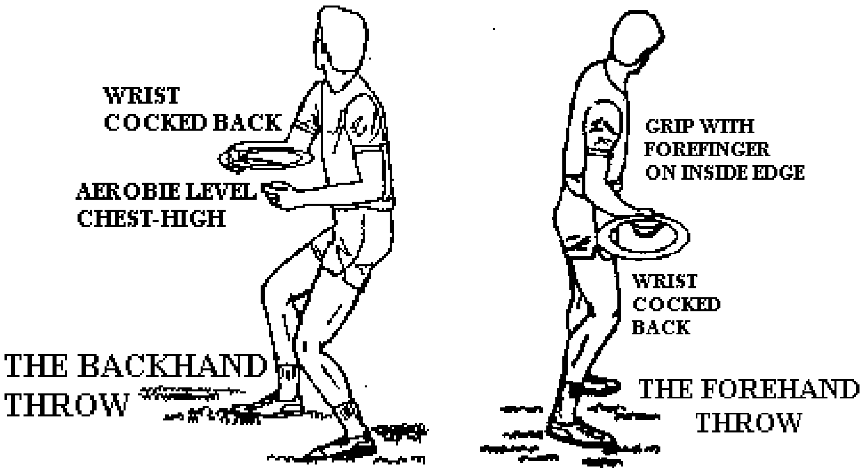

(a) Backhand

(c) Forehand

Figure 9- A couple examples of how discs were thrown (Aerobie, 2015).

Part 3: Computer Simulation

Two simulations of disc flight were created in Mathematica; the first simulated flight in two-dimensions and the second included a third dimension. In the two-dimensional model, the equations of motion corresponding with lift and drag were taken from Potts and Crowther's wind tunnel data (after comparison with my data). The three-dimensional model also took the disc spin rate and torque pitch moments into account, producing results that include the noticeable roll observed in disc flight. While similar to Hummel's procedure (1997) for computationally simulating disc flight, the drag and lift coefficient graphs were fit to polynomials of the fourth degree instead of the second for greater accuracy in these simulations.

Data Analysis

Part 1: Video Recording and Analysis

Video data for sixteen flights was analyzed with Tracker and interaction of the velocities and accelerations in various directions led to estimates of the drag and lift coefficients. The flights in our data had a small range of attack angles; the calculated lift and drag coefficients at that angle were compared with past data (table 1, fig. 9).

Table 1- Comparison of drag and lift coefficients at 11 degree angle of attack

	Potts and Crowther	My data
Drag Coefficient, $\alpha = 17^\circ$	0.45 ± 0.02	0.3 ± 0.3
Lift Coefficient, $\alpha = 17^\circ$	1.12 ± 0.05	1 ± 0.4

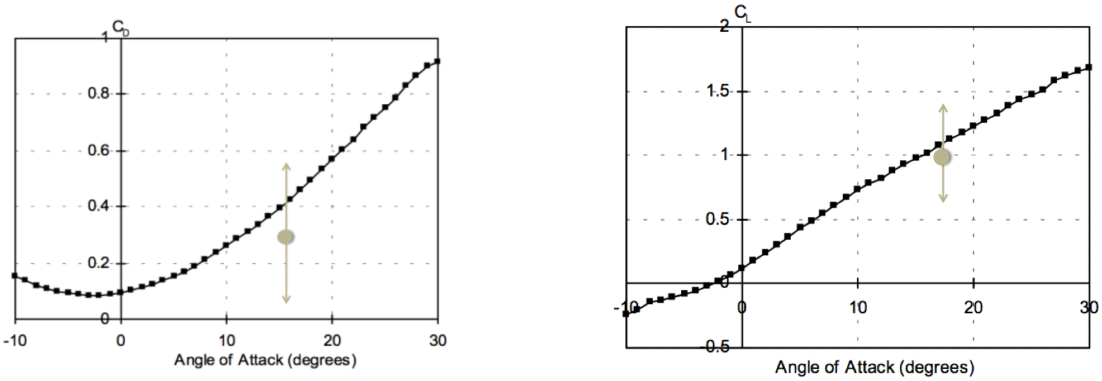

(a) Comparison of drag coefficient

(b) Comparison of lift coefficient

Figure 9- Comparison of video data with Potts & Crowther (2010) lift and drag coefficient graphs

Part 2: Calculating Lift and Drag Force Coefficients

Because the video data taken in this study matched the Potts and Crowther curves at that attack angle within reasonable error estimates, their data curves were used in calculating the lift and drag coefficients at all angles, and thus their correspondent forces.

The following equations represent the fourth-order drag and lift coefficient polynomials. They were obtained by using a CalComp2500 Digitizer on the lift and drag coefficient graphs, then plotting and fitting the function to a curve. It was more convenient for later calculations to keep the equations in terms of the sine of the attack angle. Here are the coefficient equations found from the digitized data:

Drag Coefficient Equation

$$C_D(\sin\theta) = .098577 + 0.32721 sin\theta + 3.5455(sin\theta)^2 - 0.99958(sin\theta)^3 - 1.6474(sin\theta)^4$$

Lift Coefficient Equation

$$\frac{C_L(\sin\theta)}{\cos\theta} = 0.13891 + 2.9945\sin\theta + 4.5443(\sin\theta)^2 - 16.267(\sin\theta)^3 + 19.905(\sin\theta)^4$$

Part 3: Flight Data Recorder

The data from more than twenty flights with the Flight Data Recorder were plotted and analyzed both visually and computationally. The nine-degrees of freedom FDR data was recovered for two dimensions (the symmetric x and y) of gyroscope and acceleration data, but the magnetometer data was not useful; the response rate was apparently not fast enough to keep up with the spin. z components of gyroscope and acceleration also did not give good data, as they tended to saturate during a throw.

Typically each FDR data file contained multiple flights in catch-throw-hold sequences in a continuous stream of data. The gyroscope z-component, which typically saturated during a flight, made it easy to separate the flight data from the non-flight data. Each flight segment was put into its own file and was then analyzed visually and computationally. Graphs were printed showing all nine degrees of freedom varying over time for each throw.

According to Kirkman (2014), a free body moves with:

$$\psi = -\frac{I_3 - I_1}{I_1}\omega_3 t$$

For a disc, with I_3 = 2* I_1, the x- and y- components of the gyroscope-measured omega vector rotate at a frequency of ω_z. The phase of the x and y gyroscope data was found using the following:

$$phase = arctan(\omega_y/\omega_x)$$

Discontinuities in phase, when a phase of -180 degrees was followed by a +180 degrees, were healed to make a continuous, linear phase and the slope was calculated using WAPP+. Determination of phase did not work when the x and y components were small, so this procedure was only possible for the longer throw data.

The acceleration data was also analyzed by setting x- or y- component of acceleration data from each throw against a sinusoidal function:

f(t)= k1*sin(k2*(t-a) + k3) + k4 + k5(t-a)

where *t* is time and *a* is the initial time of each throw, with parameters k1-k5 varied until the function matched the data adequately. The frequencies (values of k2) of each sinusoidal data set were used to determine the angular velocity, or spin rate, of the disc (table 2). The slight differences in frequencies from acceleration and gyroscope data may be indicators of disc wobble motion, but this was not explored thoroughly.

Table 2- Typical spin rates

Throw	Short Backhand	Short Hammer	Long Backhand	Long Forehand
Spin Rate (rad/s)	31.3 ± .2	-34 ± 2	52 ± 5	-48 ± 2

There also seemed to be an evident damping of $\omega_{xy}$for throws of longer duration (see fig 10 & 11). In the shorter flights, this phenomenon was not evident. This information is consistent with the fact that discs are spin-stabilized; higher spin rates damp the wobble faster.

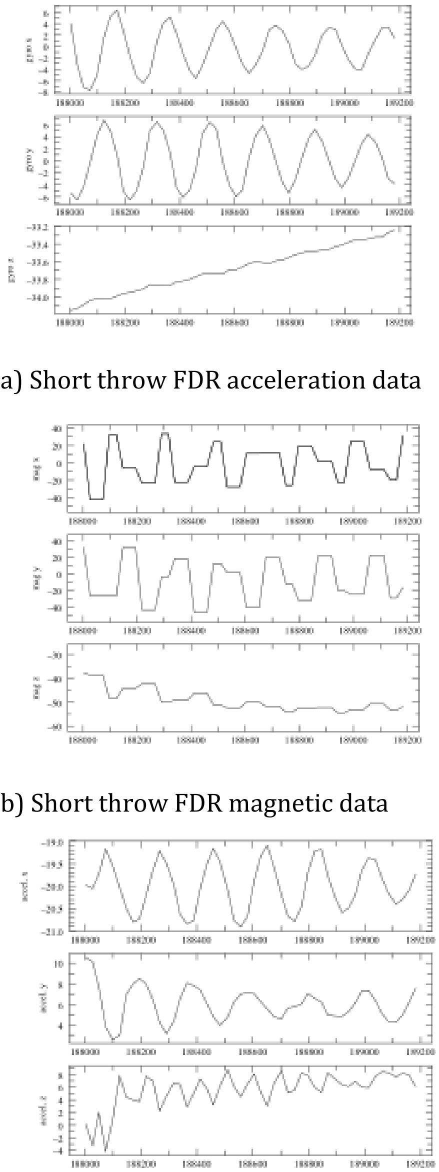

(a) Short throw FDR acceleration data

(b) Short throw FDR magnetic data

(c) Short throw FDR gyroscope data

Figure 10- Graphs of FDR Data. of a short throw (~15 yards)

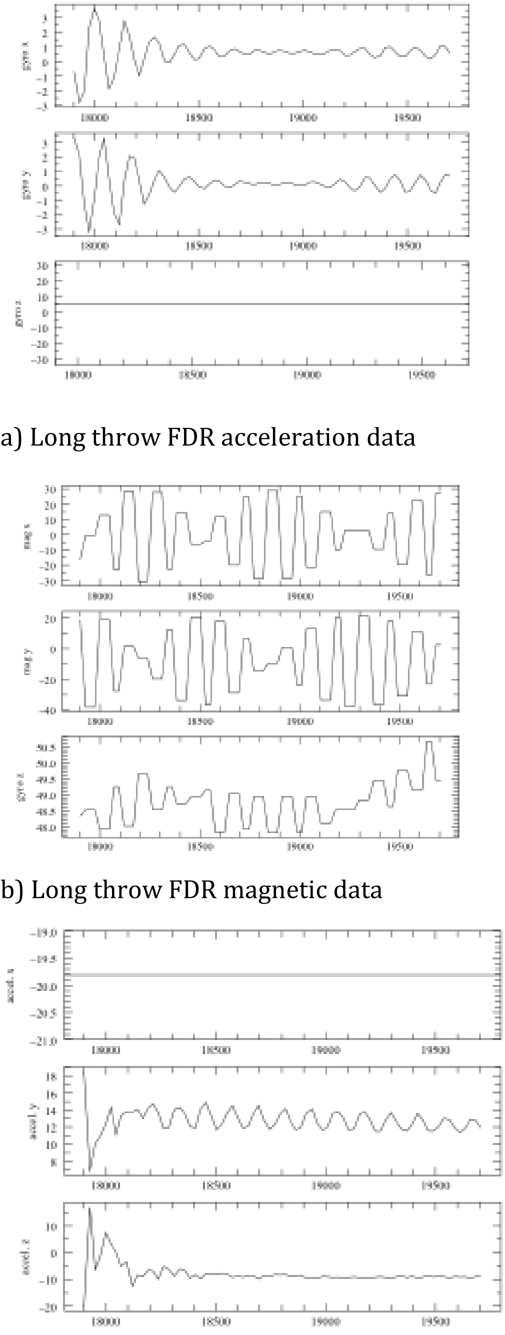

(a) Long throw FDR acceleration data

(b) Long throw FDR magnetic data

(c) Long throw FDR gyroscope data

Figure 11- Graphs of FDR Data. of a long throw (~30 yards)

Results and Discussion

Two computer simulations were written in Mathematica. The first combined the varying lift and drag forces to output information about a given flight in two dimensions. The flight patterns, in the simulation as in reality, depended on disc release angle and initial velocity. The second also included a third dimension due to the torque of wind hitting the underside of the disc. A more detailed description of the simulation setup is included in the Appendix section.

The simulations were used for specific angles of attack and initial velocities found with video and final position was compared. Graphs of position and velocity over time as well as attack angle and disc orientation give insight into the disc flight pattern. For the following (table 3, fig 12), inputs were taken from tracker results for a "far backhand throw" with initial velocity at 22 m/s at 2 degrees above horizontal and disc inclination angle of 11 degrees above horizontal.

Table 3- Large uncertainties in these values come from the uncertainty in tracker – the disc became blurry at high speeds.

Observed Distance	2D Simulation	3D Simulation
50 ± 3 m	45 ± 10 m	36 ± 15 m

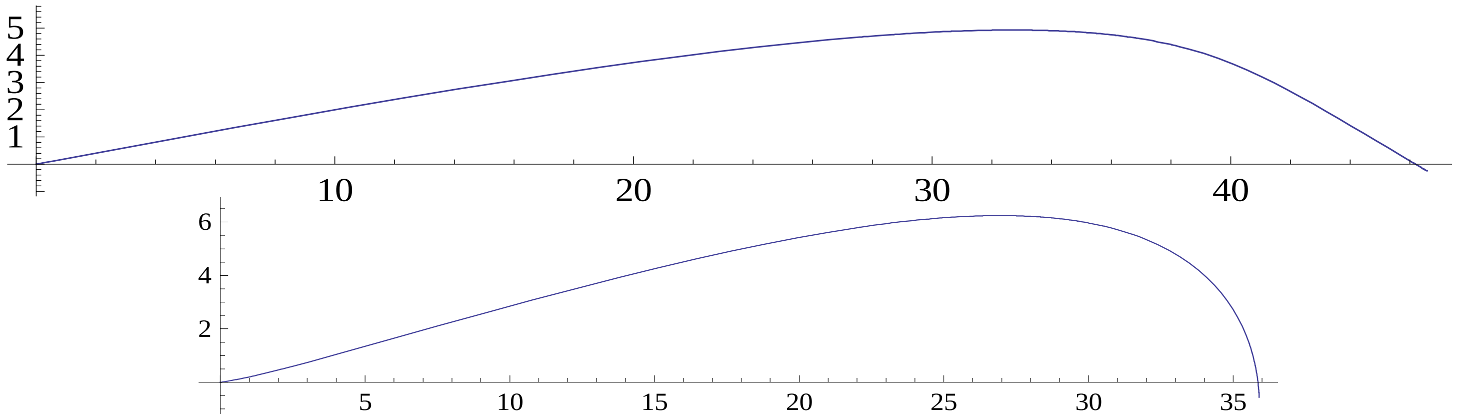

Figure 12- Simulation results of x vs z position during a flight (2D on top, 3D on bottom).

Simulations were also run for a throw of opposite spin and for a throw with a very high release angle. Throws with opposite spin followed the same flight pattern, but with the roll occurring in the opposite direction, as expected. This means that a throw released as a forehand with the same conditions (velocity, angles, absolute value of spin rate) as a backhand follows a symmetric flight pattern to that of the backhand. A high release angle (disc angle 35 degrees, release velocity angle 9 degrees) for a throw at 22 m/s was tested in each simulation. Both show a peak height of 10 m, but after the peak, the disc continues in the positive x direction in the 2D case (fig 13a) while turning back toward the thrower in the 3D approximation. The second case is, as expected, closer to what happens in reality (fig. 13b).

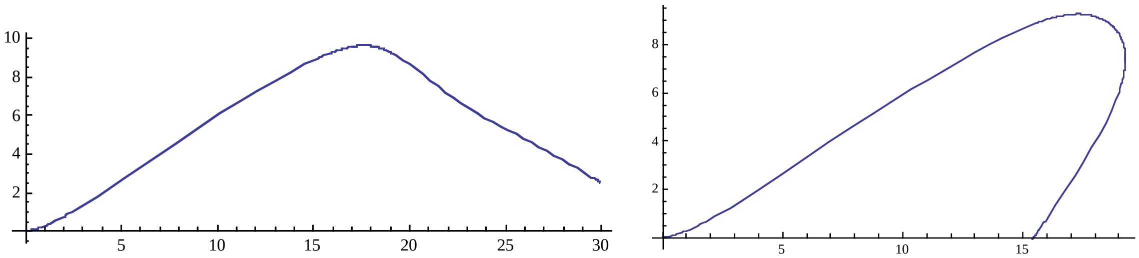

(a) 2d simulation results

(b) 3d simulation results

Figure 13- Results for a disc thrown with a very high release angle and initial velocity direction.

Applications of this model include optimizing angles in windy throwing situations, giving expected results for certain throws, and insight into the S-curve observed in certain throws. By inputting initial velocities, angle of attack and throw velocity, results change as expected. While observed throws do not match simulations perfectly, errors are present in observed velocity and angle measurements as well as measured distance. While the simulation aims to cover all aspects of forces, the drag and lift coefficients are still not fully understood and perfect conditions are not easily obtainable.

References

Bloomfield, L. A., "The flight of the frisbee." Scientific American: Vol. 280, p. 132. 1999.

Hubbard, M. & Hummel, S. A., "Simulation of frisbee flight." June 16, 2000.

Hummel, S. A., "Frisbee flight simulation and throw biomechanics." 1997.

Lorenz, R. D., "Flight and attitude dynamics measurements of an instrumented Frisbee." *Measurement Science & Technology*: Vol. 16, Number 3, p. 738-748. 2005.

Lorenz, R. D., "Flight Dynamics Measurements on an Instrumented Frisbee." November 9, 2003.

Potts, J. R. & Crowther, W. J., "Frisbee Aerodynamics." 20th AIAA Applied Aerodynamics Conference & Exhibit. June 24, 2002.

bram de vries (May 31, 2013). FreeCAD Tutorial. Youtube (Online). https://www.youtube.com/watch?v=xs1mFiJBYIo

Brown, D., "Tracker: video analysis and modeling tool." https://www.cabrillo.edu/~dbrown/tracker/

Scodary, A., "The aerodynamics and stability of flying discs." Coursework for Stanford University Physics 210, October 30, 2007. http://large.stanford.edu/courses/2007/ph210/scodary1/

Wikipedia Contributors, "Disc golf." http://en.wikipedia.org/wiki/Disc_golf Accessed- April 28, 2015.

Taylor, J., "Classical Mechanics." University Science Books. 2005.

Discraft, Inc. "Discraft Ultra-Star 175 gram ultimate sportdisc" http://www.discraft.com/ultprod.html Accessed- April 28, 2015.

Kirkman, T., "Euler angles & free precession." November, 2014.

Other picture websites:

- http://aerobie.narod.ru/images/diag-forehand-throw.gif
- http://aerobie.narod.ru/images/diag-backhand-throw.gif
- http://i228.photobucket.com/albums/ee63/Spideristic/Profiles%20in%20History%20-%20Auction%2042/Lot63_bttf3_frisbes_pies_plate.jpg
- https://i0.wp.com/www.sikhnet.com/files/news/2008/September/pic-3.jpg
- http://viresethonestas.com/wp-content/uploads/2014/12/Olympics_discus.jpg
- http://www.mnn.com/sites/default/files/styles/featured_blog/public/wfm-feat.jpg
- http://www.boomerbookofchristmas.com/wham-o-an-early-history/lens4410782_1241705439wham-o_frisbee/
- https://wlurecreation.wordpress.com/2011/05/18/disc-golf-tournament-on-friday-come-on-take-break-from-studying/
- http://mathworld.wolfram.com/EulerAngles.html

Acknowledgements:

I would like to express my gratitude to my advisor, Dr. Thomas Kirkman, for his countless hours of work and personal lectures on this topic. I would also like to thank him for his help with entering formulas into the mathematica program and his Flight Data Recorder design.

I would also like to thank all of the students who helped me take data: John Schwend, Lexi Bernstein, Andrew Honzay, Charlotte Waterhouse, Lauren Lingenfelter, Alex Daggett, Meghan Hayden, Aaron Wildenborg, Patrick Ellingson, Raul Vargas, and Luke Loso.

Appendix:
Mathematica Code and Explanations

2 d (1 st approx)

```
m = .175;
g = 9.8;
r = .27305/2;
A = Pi r^2;
rho = 1.2041;
```

→ Defining constants

```
K1 = .09857432; K2 = .3272530; K3 = 3.545699; K4 = -1.001032; K5 = -1.645254;
CD[x_] = K1 + K2*x + K3*x^2 + K4*x^3 + K5*x^4;
L1 = .1389740; L2 = 2.991266; L3 = 4.443459; L4 = -17.41488; L5 = 18.42772;
CL[x_] = L1 + L2*x + L3*x^2 + L4*x^3 + L5*x^4;
```

→ Defining lift and drag coefficient equations

```
v = {x'[t], 0, z'[t]};
nv = Sqrt[x'[t]^2 + z'[t]^2];
phi = Pi;
```

→ Defining velocity (2d), speed (length of velocity vector) and phi angle

```
n = {Sin[theta] Cos[phi], Sin[theta] Sin[phi], Cos[theta]};
```

→ Defining the disc normal vector

```
Lift = Simplify[.5 A rho CL[-Dot[v, n]/nv] Cross[Cross[v, n], v]];
Drag = -.5 A rho v nv CD[-Dot[v, n]/nv];
rhs = Lift + Drag + {0, 0, -m g};
```

→ Defining force equations

```
theta = Pi/180 * 35;
theta0 = Pi/180.*9;
v0 = 22;
```

→Input variables theta0 here is velocity angle, theta is disc angle

```
solution =
  NDSolve[{x''[t] == rhs[[1]]/m, z''[t] == rhs[[3]]/m, x[0] == 0, z[0] == 0,
   z'[0] == v0 Sin[theta0], x'[0] == v0 Cos[theta0]}, {x, z}, {t, 0, 10}];
```

→ Solving the differential equations for accelerations/forces

List of possible plots:

```
ParametricPlot[Evaluate[{x[t], z[t]} /. First[solution]], {t, 0, 5.5},
 PlotRange -> All]
```

→ Plot of x vs z distance (side-view)

```
Plot[Evaluate[{ArcSin[-Dot[v.n]/nv]*180/Pi} /. First[solution]], {t, 0, 5},
 PlotRange -> All]
```

→ Plot of angle of attack vs time

```
Plot[Evaluate[z[t] /. First[solution]], {t, 0, 5.5}, PlotRange -> All,
 AspectRatio -> .2]
ParametricPlot[Evaluate[{x'[t], z'[t]} /. First[solution]], {t, 0, 5},
 PlotRange -> All, AspectRatio -> Automatic]
```

→ Plot of x vs z velocities

```
t0 = 7.0;
Evaluate[{x'[t0], z'[t0]} /. First[solution]]
Evaluate[{x[t0], z[t0]} /. First[solution]]
```

→ Gives the x and y velocity and position for a given input time

3 d (2 nd approx)

```
m = .175;
g = 9.8;
r = .27305/2;
A = Pi r^2;
rho = 1.2041;
I3 = .5 m r^2;
I1 = I3/2;
```

→ Inputting constants

```
v0 = 22;
theta0 = 9*Pi/180;
spin = 50;
thetad = 35*Pi/180;
```

→Input variables: velocity and angle of velocity(radians) at t0, spin rate (rad/s) and release angle at t0

```
v = {x'[t], y'[t], z'[t]};
nv = Sqrt[x'[t]^2 + y'[t]^2 + z'[t]^2];
n = {Sin[theta[t]] Cos[phi[t]], Sin[theta[t]] Sin[phi[t]], Cos[theta[t]]};
```

→ Defining velocity, the scalar speed, and the disc normal vector)

```
K1 = .09857432; K2 = .3272530; K3 = 3.545699; K4 = -1.001032; K5 = -1.645254;
CD[x_] = K1 + K2*x + K3*x^2 + K4*x^3 + K5*x^4;
L1 = .1389740; L2 = 2.991266; L3 = 4.443459; L4 = -17.41488; L5 = 18.42772;
CL[x_] = L1 + L2*x + L3*x^2 + L4*x^3 + L5*x^4;
```

→Defining lift and drag coefficient equations

```
Lift = Simplify[.5 A rho CL[-Dot[v, n]/nv] Cross[Cross[v, n], v]];
Drag = -.5 A rho v nv CD[-Dot[v, n]/nv];
rhs = Lift + Drag + {0, 0, -m g};
```

→ Defining force equations)

```
mphi = {{Cos[phi[t]], -Sin[phi[t]], 0}, {Sin[phi[t]], Cos[phi[t]], 0}, {0, 0,
   1}};
mtheta = {{Cos[theta[t]], 0, Sin[theta[t]]}, {0, 1, 0}, {-Sin[theta[t]], 0,
   Cos[theta[t]]}};
```

→ Defining transformation matrices. The working frame requires only two transformations (no psi matrix) and is in the disc plane but does not spin with the disc.

```
{0, theta'[t], 0} + Inverse[mtheta].{0, 0, phi'[t]};
Simplify[%];
wb = %;
{0, 0, dpsi[t]} + {0, theta'[t], 0} + Inverse[mtheta].{0, 0, phi'[t]};
Simplify[%];
wpb = %;
Lpb = {{I1, 0, 0}, {0, I1, 0}, {0, 0, I3}}.wpb;
```

→ Defining frames. wb is omega of our frame (disc wobble), wpb is the omega of the disc in the frame (disc spin rate) and Lpb is the angular momentum of the disc in the frame we are using)

```
Trhs = Simplify[D[Lpb, t] + Cross[wb, Lpb]];
torque = Simplify[.5 A rho nv 2 r*
   Cross[Inverse[mtheta].Inverse[mphi].v, {0, 0, 1}]*pm[-Dot[v, n]/nv]];
k1 = -.009204492; k2 = .07469542; k3 = -.2275474; k4 = 1.853262; k5 = -1.191175;
pm[x_] = k1 + k2*x + k3*x^2 + k4*x^3 + k5*x^4;
```

→ These are the torque equations. They involve the pitch moment coefficient.

```
solution =
  NDSolve[{torque[[1]] == Trhs[[1]], torque[[2]] == Trhs[[2]],
   torque[[3]] == Trhs[[3]], phi[0] == Pi, theta[0] == thetad,
   dpsi[0] == spin, phi'[0] == 0, theta'[0] == 0, x''[t] == rhs[[1]]/m,
   y''[t] == rhs[[2]]/m, z''[t] == rhs[[3]]/m, x[0] == 0, y[0] == 0,
   z[0] == 0, z'[0] == v0 Sin[theta0], x'[0] == v0 Cos[theta0],
   y'[0] == 0}, {x, y, z, phi, theta, dpsi}, {t, 0, 10}, MaxSteps -> 20000];
```

→Solving the force and torque differential equations with initial conditions specified.

List of possible plots:

```
ParametricPlot[Evaluate[{x[t], z[t]} /. First[solution]], {t, 0, 4},
 PlotRange -> All]
```

Plot of x vs z position (as if viewing from the side)

```
ParametricPlot[Evaluate[{x[t], y[t]} /. First[solution]], {t, 0, 5},
 PlotRange -> All]
ParametricPlot[Evaluate[{y[t], z[t]} /. First[solution]], {t, 0, 5},
 PlotRange -> All]
Plot[Evaluate[{z[t]} /. First[solution]], {t, 0, 5}, PlotRange -> All]
Plot[Evaluate[{y[t]} /. First[solution]], {t, 0, 2.3}, PlotRange -> All]
```

Plot of y position vs time (as if viewing as if from the thrower's position)

```
Plot[Evaluate[{x[t]} /. First[solution]], {t, 0, 5}, PlotRange -> All]
ParametricPlot[Evaluate[{x[t], y[t]} /. First[solution]], {t, 0, 5},
 PlotRange -> All]
```

Plot of x vs y position (as if viewing from above)

```
Plot[Evaluate[{ArcSin[-Dot[v, n]/nv]*180/Pi} /. First[solution]], {t, 0, 5},
 PlotRange -> All]
```

```
Inverse[mtheta].Inverse[mphi] /. t -> t0;
ParametricPlot[
 Evaluate[{Sin[theta[t]] Cos[phi[t]], Sin[theta[t]] Sin[phi[t]]} /.
   First[solution]], {t, 0, t0}, PlotRange -> All]
Plot[Evaluate[Sin[theta[t]] Sin[phi[t]] /. First[solution]], {t, 0, t0},
 PlotRange -> All]
```

```
t0 = 4;
```

→ Input variable: pick a time near the end of the flight

```
Evaluate[{x[t0], y[t0], z[t0]} /. First[solution]]
{x'[t0], y'[t0], z'[t0]} /. First[solution]
{Sin[theta[t0]] Cos[phi[t0]], Sin[theta[t0]] Sin[phi[t0]], Cos[theta[t0]]} /.
 First[solution]
{theta[t0], phi[t0]} /. First[solution]
Evaluate[ArcSin[
   Evaluate[-Dot[{x'[t], y'[t], z'[t]}/Sqrt[x'[t]^2 + y'[t]^2 + z'[t]^2],
      n] /. First[solution]]] 180/Pi /. t -> t0]
```

→ These numbers represent:

-distance in (x, y, z)
-velocities in (x, y, z) at t0,
-orientation of the disc (disc normal vector) at t0,
-another form of disc orientation